PNAS
www.pnas.org

Supplementary Information for

Soluble CX3CL1 gene therapy improves cone survival and function in mouse models of retinitis pigmentosa

Sean K. Wang, Yunlu Xue, Parimal Rana, Christin M. Hong, Constance L. Cepko

Constance L. Cepko
Email: cepko@genetics.med.harvard.edu

This PDF file includes:

SI Materials and Methods
Figs. S1 to S6
Tables S1 to S3
References for SI reference citations

www.pnas.org/cgi/doi/10.1073/pnas.1901787116

SI Materials and Methods

AAV production and purification

Recombinant AAV serotype 8 (AAV8) vectors were generated as previously described (1, 2). HEK293T cells were transfected using polyethylenimine with a mixture of the AAV plasmid, rep2/cap8 packaging plasmid, and adenovirus helper plasmid. Seventy-two hours post-transfection, the supernatant was harvested and viral particles precipitated by overnight PEGylation followed by centrifugation. To remove cell debris, viruses were then subjected to centrifugation through an iodixanol gradient. The recovered AAV was washed three times with PBS and concentrated to a final volume of 100-200 µl. The titer of purified AAVs was semi-quantitatively determined by staining of viral capsid proteins VP1, VP2, and VP3 using SYPRO Ruby (Molecular Probes) and relating the staining intensity to a standard AAV titered using RT-PCR of genome sequences.

Subretinal AAV delivery

All AAV injections were performed on P0-P1 neonatal mice. Following anesthetization of the mouse on ice, the palpebral fissure was carefully cut using a 30-gauge needle and the eye exposed with dull forceps. A glass needle controlled by a FemtoJet microinjector (Eppendorf) was then used to deliver a volume of ~0.25 µl into the subretinal space for all injections. To standardize labeling of cones, AAV8-GFP and AAV8-mCherry were administered at $5x10^8$ vector genomes (vg) per eye, a dose adequate for infecting >90% of cones in WT retinas (*SI Appendix*, Fig. S1). All other vectors were dosed at $1x10^9$ vg per eye. Recently, we reported dose-dependent toxicity with some AAV vectors independent of protein expression, capsid serotype, or preparation method (3). Because retinas infected with both AAV8-GFP and a therapy candidate received a higher dose of total virions, we would predict any vector-induced toxicity in these samples to be greater than in control eyes.

The subretinal bleb was formed in the inferotemporal quadrant for the right eye and superotemporal quadrant for the left. Right and left eye injections for each condition were alternated from litter to litter, and no significant difference was found in the number or distribution of GFP-positive cones between right or left eyes injected with the same AAV mixture.

RPE explants

Enucleated eyes were dissected in PBS to remove the cornea, iris, lens, ciliary body, retina, and connective tissue. Four relaxing radial incisions were made to the remaining RPE-choroid-sclera complex. Each complex was then placed on a 12 mm Millicell cell culture insert (Millipore) resting on 3 mL of prewarmed culture media with the RPE side facing up. Culture media consisted of a 1:1 ratio of DMEM and F-12 supplemented with L-glutamine, B27, N2, and penicillin-streptomycin. Explants were maintained in humidified incubators at 37°C and 5% CO2 for 48 hours, after which the media was collected and assayed for CX3CL1 protein using a commercial ELISA kit (R&D Systems) according to manufacturer's instructions. ELISA reactions were performed in duplicate using 50 µl of media as input.

Image acquisition and analysis

GFP-positive cones in flat-mounted retinas were quantified using a custom ImageJ module. To indicate the location of the optic nerve head and boundaries of the retina, a line was first drawn by the user from the optic nerve head to the center of the edge of each of the four retinal leaflets as depicted in *SI Appendix*, Fig. S2. All subsequent steps were performed by the module without requiring user input. To define the region corresponding to the central retina, the module connected the four aforementioned lines at their midpoints to form a quadrilateral around the optic nerve head. The image then underwent several processing steps to account for areas of uneven fluorescence or overlapping GFP signal, including local background subtraction, watershed segmentation, and particle size filtering. Finally, an automatic threshold was applied, and the number of GFP-positive particles within the quadrilateral was quantified by the module. This value was used to represent the number of GFP-positive cones in the central retina of the sample. The module can be freely downloaded from https://sites.imagej.net/Seankuwang/.

Electroretinography (ERG)
To minimize inter-animal variation, conditions were tested using right and left eyes of the same animals. Mice were dark-adapted overnight and anesthetized with an intraperitoneal injection of 100 mg/kg ketamine and 10 mg/kg xylazine. Following dilation of the pupils with 1% tropicamide, gold-wire electrodes were applied to the surface of both eyes and hydrated with a drop of lubricating gel (Optixcare). Reference and ground electrodes were placed subcutaneously near the scalp and tail, respectively. The animal was then light-adapted for 12 minutes under a 30 cd/m^2 background light. Upon completion of light adaptation, photopic vision was assessed using multiple flashes of 1, 10, and 100 cd/m^2 light. The average amplitude of the photopic b-wave in response to each flash intensity was subsequently measured by an observer blinded to the treatment assignment.

Optomotor assay
Mice were placed on a platform within a virtual-reality chamber in which the spatial frequency of a displayed sine wave grating could be altered using a computer program. A bright background luminance setting was used to saturate rod responses to provide a measure of cone vision. During each test, an observer blinded to the treatment assignment assessed for reflexive head-tracking movements in response to the grating stimulus. Right and left eyes were tested independently using counterclockwise and clockwise gratings, respectively, as only motion in the temporal-to-nasal direction evokes the optomotor response in mice (4). For each eye, the highest spatial frequency at which the animal tracked the grating was determined to be the visual acuity.

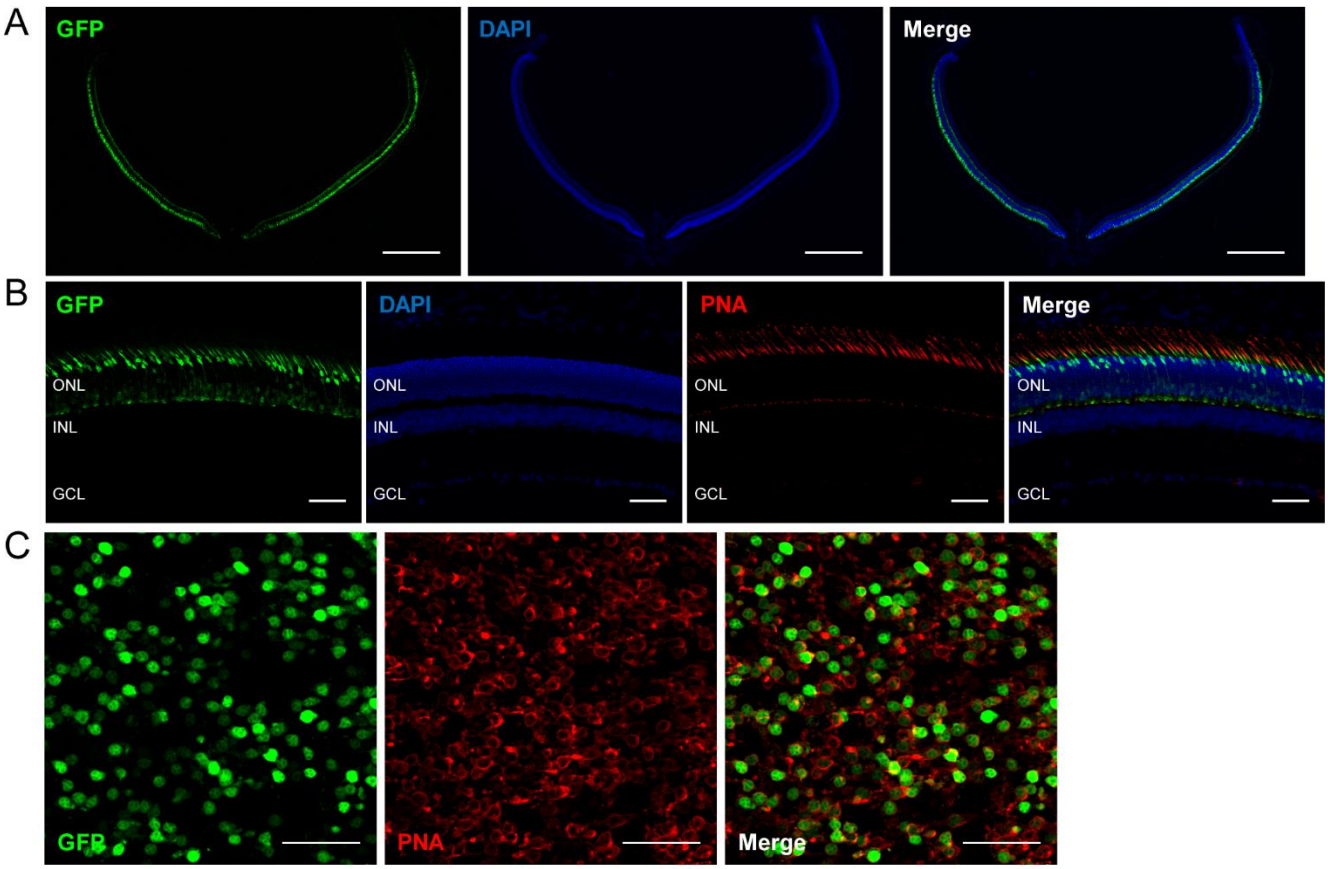

Fig. S1. Expression of AAV8-GFP in cone photoreceptors. (**A**, **B**) Cross-section from a P50 WT (CD-1) retina infected at P0-P1 with $5x10^8$ vg of AAV8-GFP and stained with peanut agglutinin lectin (PNA), a marker of the matrix surrounding cone inner and outer segments (5). Scale bars, 500 µm (A), 50 µm (B). (**C**) High-magnification image of a flat-mounted P50 WT retina infected at P0-P1 with AAV8-GFP and stained with PNA. Scale bar, 20 µm.

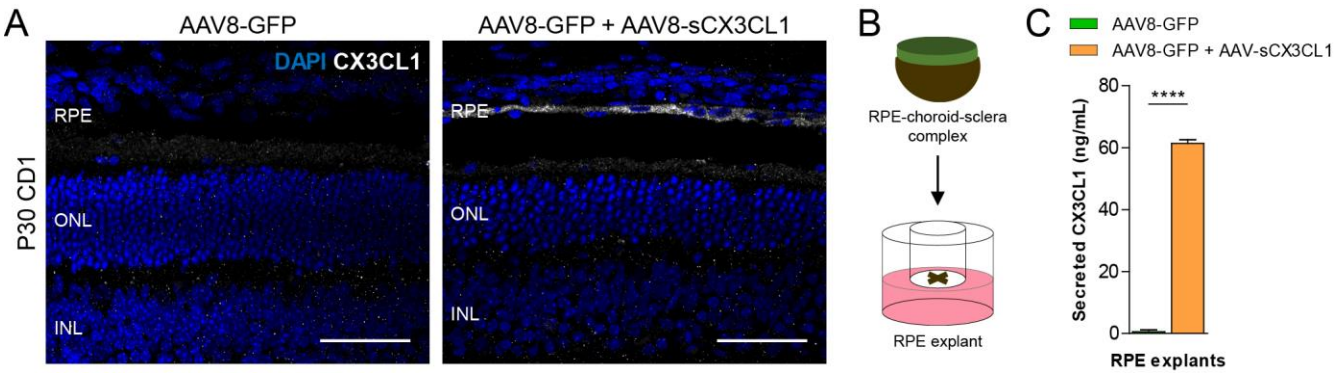

Fig. S2. Validation of sCX3CL1 overexpression with AAV8-sCX3CL1. (**A**) Cross-section from a P30 WT (CD-1) retina infected at P0-P1 with AAV8-GFP or AAV8-GFP plus AAV8-sCX3CL1 and stained with anti-CX3CL1 antibody. Scale bar, 50 µm. (**B**) Schematic of RPE explant culture. The RPE-choroid-sclera complex was isolated from the rest of the eye and placed on a cell culture insert resting on culture media. (**C**) Quantification of secreted CX3CL1 from P40 WT RPE extracts infected at P0-P1 with AAV8-GFP or AAV8-GFP plus AAV8-sCX3CL1. Media was collected 48 hours after explantation and assayed by ELISA. RPE, retinal pigment epithelium; ONL, outer nuclear layer; INL, inner nuclear layer.

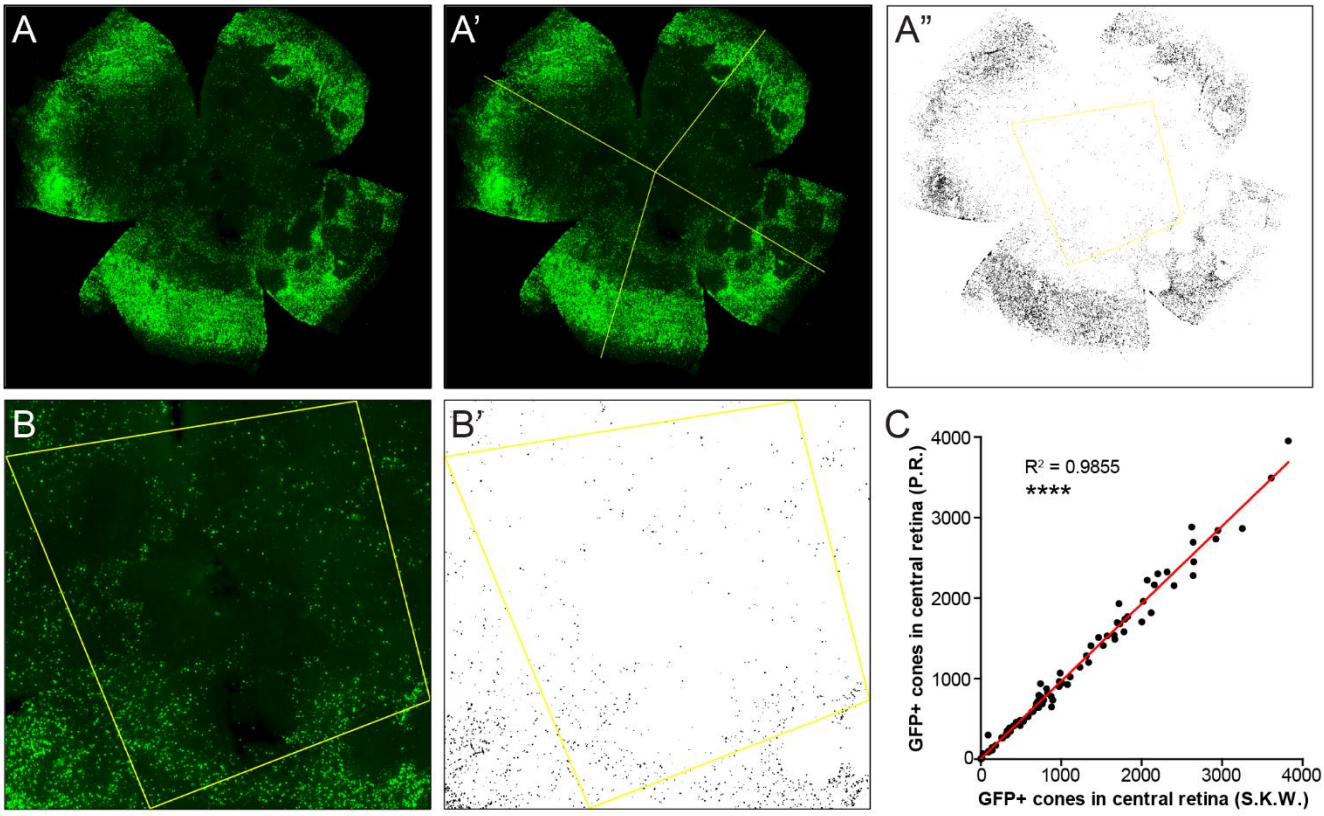

Fig. S3. Cone quantification methodology. (**A**) Representative image of a P50 flat-mounted RP retina infected at P0-P1 with $5x10^8$ vg of AAV8-GFP to label cones. (**A'**) A line was drawn by the user from the optic nerve head to the center of the edge of each of the four retinal leaflets. (**A"**) An ImageJ module then subjected the image to automatic processing and thresholding, connected the midpoints of these four lines to form a region defined as the central retina, and quantified the number of GFP-positive cones in the central retina. (**B**, **B'**) Comparison of raw image from a flat-mounted RP retina infected with AAV8-GFP versus the same retina after automatic processing and thresholding. (**C**) Correlation of cone quantification results obtained independently by two authors (S.K.W. and P.R.) using the ImageJ module. Each dot (n = 87) represents a separate retina. **** P<0.0001. R^2 determined using Pearson's correlation analysis.

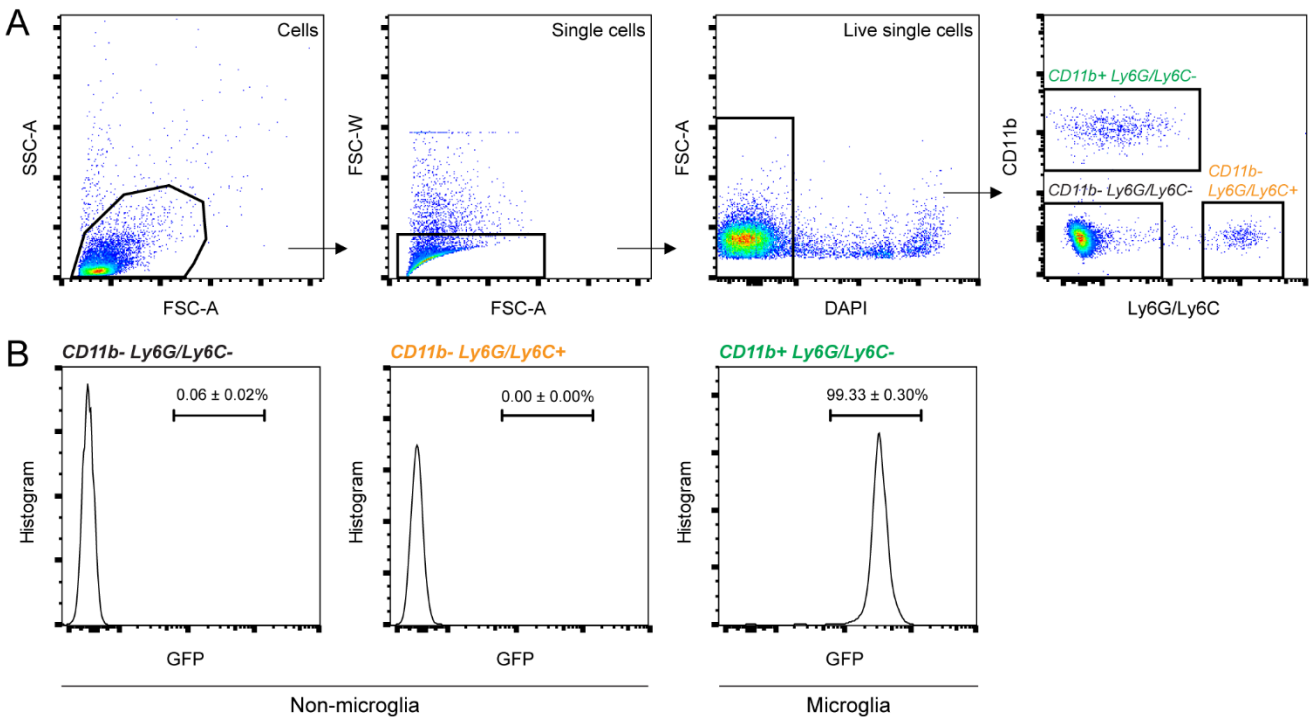

Fig. S4. Flow cytometry gating of retinal microglia. (A) P35 *rd1*;Cx3cr1$^{GFP/+}$ retinas were dissociated and gated for DAPI-negative single cells, from which three populations were isolated. (**B**) Histograms of Cx3cr1^{GFP} signal in each population. CD11b+ Ly6G/Ly6C- cells were defined as microglia while CD11b- Ly6G/Ly6C- and CD11b- Ly6G/Ly6C+ cells were defined as non-microglia. Data shown as mean ± SEM. *n* = 4 animals per condition.

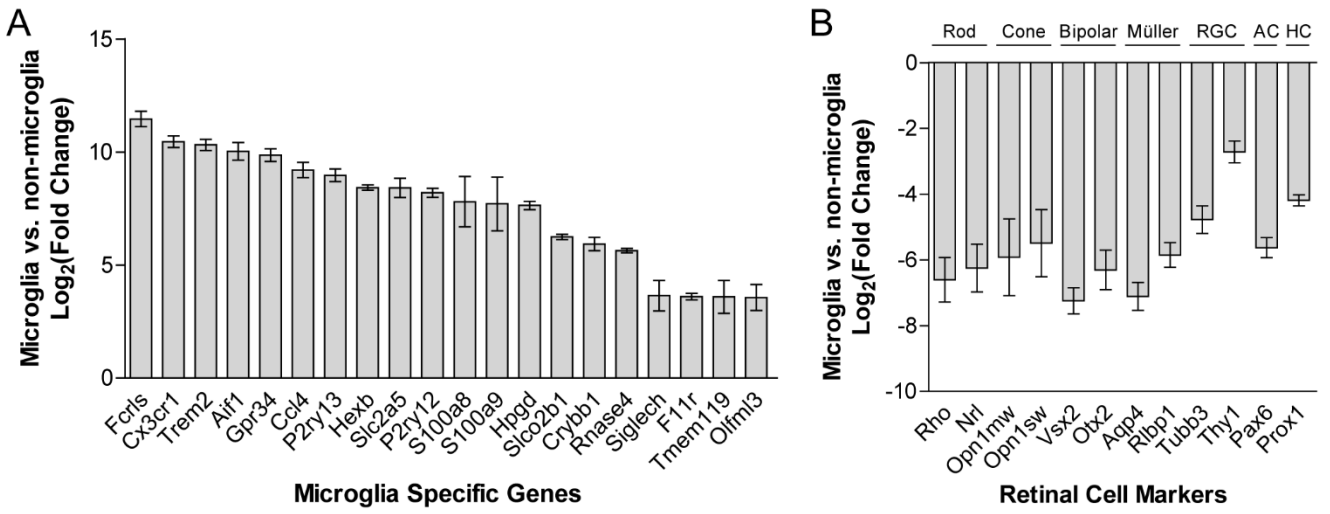

Fig. S5. Microglia and retinal cell markers in sorted cell populations. (**A**) Comparison of microglia and non-microglia cell populations sorted from *rd10* retinas for expression of 20 microglia-specific genes by RNA-seq (6). (**B**) Comparison of microglia and non-microglia cell populations sorted from *rd10* retinas for expression of indicated retinal cell-type markers by RNA-seq (7–12). Data shown as mean ± SEM. *n* = 24 animals for microglia, *n* = 6 animals for non-microglia. RGC, retinal ganglion cell; AC, amacrine cell; HC, horizontal cell.

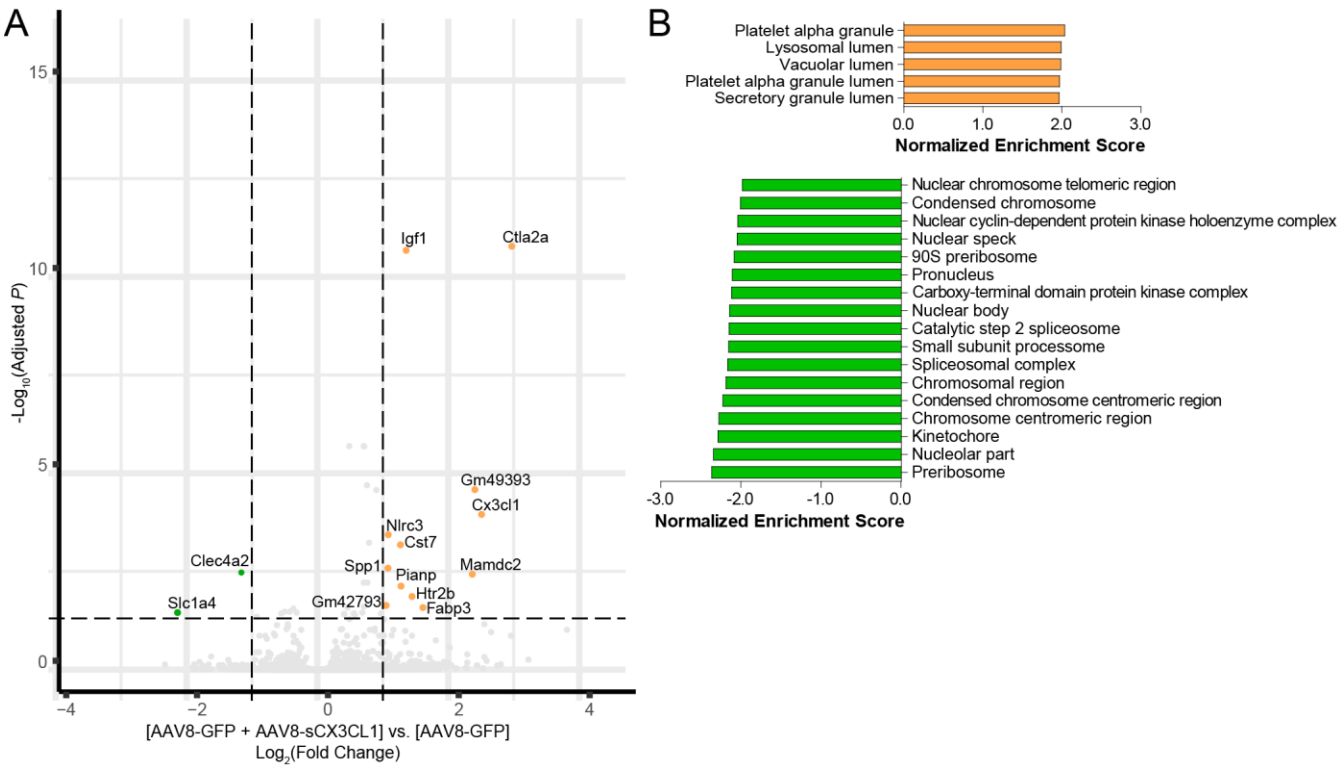

Fig. S6. Transcriptional profiling of retinal microglia during rod degeneration following sCX3CL1 overexpression. (**A**) Volcano plot of upregulated and downregulated genes from P20 *rd10* retinal microglia following infection at P0-P1 with AAV8-GFP or AAV8-GFP plus AAV8-sCX3CL1. Dotted lines indicate adjusted P<0.05 and magnitude of fold change ≥2. (**B**) Gene set enrichment analysis of P20 *rd10* microglia from retinas infected with AAV8-GFP plus AAV8-sCX3CL1 (orange) compared to AAV8-GFP alone (green). Gene sets with family-wise error rate (FWER) <0.05 are displayed. *n* = 8 animals per condition.

Table S1. RT-PCR primers.

Gene name	*5'*	*3'*
C1qa	AAAGGCAATCCAGGCAATATCA	TGGTTCTGGTATGGACTCTCC
Cd4	AGGTGATGGGACCTACCTCTC	GGGGCCACCACTTGAACTAC
Cd5l	CAGGCTGGAACTTACAGGTCT	GTCCTTTGCCCTGAGTATTCTTG
Cd68	TGTCTGATCTTGCTAGGACCG	GAGAGTAACGGCCTTTTTGTGA
Cd8a	CCGTTGACCCGCTTTCTGT	CGGCGTCCATTTTCTTTGGAA
Cst7	CCTGCCTTGAAGCGGACTC	CACCTCAAAACTGTGGAGCCA
Gapdh	AGGTCGGTGTGAACGGATTTG	TGTAGACCATGTAGTTGAGGTCA
Igf1	CCGAGGGGCTTTTACTTCAACAA	CGGAAGCAACACTCATCCACAA
Il1a	CGAAGACTACAGTTCTGCCATT	GACGTTTCAGAGGTTCTCAGAG
Il1b	GCAACTGTTCCTGAACTCAACT	ATCTTTTGGGGTCCGTCAACT
Il6	TAGTCCTTCCTACCCCAATTTCC	TTGGTCCTTAGCCACTCCTTC
Ly6g	GACTTCCTGCAACACAACTACC	ACAGCATTACCAGTGATCTCAGT
Spp1	AGCAAGAAACTCTTCCAAGCAA	GTGAGATTCGTCAGATTCATCCG
Tmem119	CCTACTCTGTGTCACTCCCG	CACGTACTGCCGGAAGAAATC
Tnf	CCCTCACACTCAGATCATCTTCT	GCTACGACGTGGGCTACAG

Table S2. Significantly upregulated genes in P70 *rd10* microglia following sCX3CL1 overexpression.

Gene	*Log_2(Fold Change)*	*Adjusted P*
Cd5l	3.29	0.000
Ryr3	3.08	0.038
Hpse	2.52	0.002
Gpnmb	2.48	0.000
Foxp2	2.38	0.025
Mcoln3	2.31	0.003
Ctla2a	2.29	0.003
Gm21188	2.26	0.000
Muc16	2.24	0.029
N4bp3	1.91	0.000
Gm4117	1.86	0.047
Cst7	1.78	0.000
Fabp5	1.75	0.000
Lrrc27	1.62	0.004
Ahnak2	1.61	0.003
Gm1673	1.58	0.000
Ifi208	1.53	0.027
Ifit3	1.49	0.015
Ikbke	1.48	0.002
Tmem82	1.42	0.023
Ldlrad3	1.42	0.000
Apoc4	1.41	0.000
Gla	1.41	0.000
Ifit3b	1.35	0.044
Ifi206	1.31	0.000
Gm5431	1.29	0.001
Slfn5	1.26	0.000
Lgals1	1.26	0.001
Ifit2	1.26	0.024
Lgals3bp	1.22	0.000
Csf1	1.22	0.000
Igf1	1.17	0.000
Lyz1	1.16	0.000
Spp1	1.13	0.009
Vnn3	1.13	0.044
Cd200r4	1.13	0.000
Zbp1	1.09	0.002
Lyz2	1.08	0.000
Rab7b	1.07	0.031
Fcrl1	1.07	0.000
Irf7	1.05	0.002
Rnf145	1.04	0.007
Rtp4	1.04	0.002
Gm42836	1.04	0.017
Oasl2	1.03	0.000
Gyg	1.03	0.000
Vat1	1.03	0.046
Mrgpre	1.03	0.027
Samd9l	1.02	0.003
Cd63-ps	1.00	0.006

Table S3. Significantly downregulated genes in P70 *rd10* microglia following sCX3CL1 overexpression.

Gene	*Log_2(Fold Change)*	*Adjusted P*
Ankrd33	-3.97	0.008
Aipl1	-3.68	0.006
Pde6g	-3.57	0.004
Chrnb4	-3.54	0.038
Gnb3	-3.36	0.005
Clca1	-3.14	0.017
Pygm	-3.13	0.008
Pdc	-3.08	0.040
Prom1	-2.97	0.049
Grk1	-2.97	0.036
Cckbr	-2.77	0.048
G730003C15Rik	-2.74	0.008
Mylk	-2.74	0.002
Kcnh6	-2.56	0.047
Rhpn2	-2.54	0.034
Iqcn	-2.41	0.000
Map1b	-2.39	0.000
Gm23849	-2.37	0.003
Syt1	-2.31	0.008
Impdh1	-2.21	0.010
Guca1a	-2.13	0.007
Mtcl1	-2.05	0.001
Gm45838	-1.89	0.016
Gm26656	-1.78	0.018
Gm44067	-1.78	0.018
Meg3	-1.65	0.045
Ncs1	-1.62	0.006
Il7r	-1.60	0.002
Gp9	-1.55	0.000
Car2	-1.48	0.035
Olfm4	-1.40	0.001
Tmc7	-1.38	0.022
S1pr4	-1.34	0.004
Tubb2b	-1.11	0.006
Gabbr1	-1.06	0.003
Dnajb13	-1.05	0.001
3110080O07Rik	-1.03	0.049
Ssbp3	-1.01	0.002
Chst7	-1.01	0.001
Adamts1	-1.00	0.004

References

1. Xiong W, Garfinkel AEM, Li Y, Benowitz LI, Cepko CL (2015) NRF2 promotes neuronal survival in neurodegeneration and acute nerve damage. *J Clin Invest* 125(4):1433–1445.
2. Grieger JC, Choi VW, Samulski RJ (2006) Production and characterization of adeno-associated viral vectors. *Nat Protoc* 1(3):1412–28.
3. Xiong W, et al. (2019) AAV cis-regulatory sequences are correlated with ocular toxicity. *Proc Natl Acad Sci U S A*. doi:10.1073/PNAS.1821000116.
4. Douglas RM, et al. (2005) Independent visual threshold measurements in the two eyes of freely moving rats and mice using a virtual-reality optokinetic system. *Vis Neurosci* 22(5):677–84.
5. Kawano K, Uehara F, Sameshima M, Ohba N (1984) Binding sites of peanut agglutinin in mammalian retina. *Jpn J Ophthalmol* 28(3):205–14.
6. Hickman SE, et al. (2013) The microglial sensome revealed by direct RNA sequencing. *Nat Neurosci* 16(12):1896–1905.
7. Akimoto M, et al. (2006) Targeting of GFP to newborn rods by Nrl promoter and temporal expression profiling of flow-sorted photoreceptors. *Proc Natl Acad Sci U S A* 103(10):3890–5.
8. Shekhar K, et al. (2016) Comprehensive Classification of Retinal Bipolar Neurons by Single-Cell Transcriptomics. *Cell* 166(5):1308–1323.e30.
9. Roesch K, et al. (2008) The transcriptome of retinal Müller glial cells. *J Comp Neurol* 509(2):225–38.
10. Chintalapudi SR, et al. (2017) Isolation of Primary Murine Retinal Ganglion Cells (RGCs) by Flow Cytometry. *J Vis Exp* (125):e55785.
11. Cherry TJ, Trimarchi JM, Stadler MB, Cepko CL (2009) Development and diversification of retinal amacrine interneurons at single cell resolution. *Proc Natl Acad Sci U S A* 106(23):9495–500.
12. Dyer MA, Livesey FJ, Cepko CL, Oliver G (2003) Prox1 function controls progenitor cell proliferation and horizontal cell genesis in the mammalian retina. *Nat Genet* 34(1):53–58.